Submitted to the *Journal of Biomechanics-Berlin Workshop*, May 2016 (BM-D-17-00168R1)

Effects of Motion Segment Simulation and Joint Positioning on Spinal Loads in Trunk Musculoskeletal Models

F. Ghezelbash[1], A.H. Eskandari[2], A. Shirazi-Adl[1], N. Arjmand[2], Z. El-Ouaaid[3], A. Plamondon[3]

[1]Division of Applied Mechanics, Department of Mechanical Engineering, Ecole Polytechnique, Montréal, Canada

[2]Department of Mechanical Engineering, Sharif University of Technology, Tehran, Iran

[3]Institut de recherche Robert Sauvé en santé et en sécurité du travail, Montréal, Canada

Abstract word count: 256

Manuscript word count: ~4350

Corresponding Author:

Farshid Ghezelbash, Department of Mechanical Engineering, Ecole Polytechnique, Montreal, Quebec, Canada.

Email: ghezelbash.far@gmail.com

Telephone: (514) 340-4711 Ext. 4129

Abstracts

Musculoskeletal models represent spinal motion segments by spherical joints/beams with linear/nonlinear properties placed at various locations. We investigated the fidelity of these simplified models (i.e., spherical joints with/without rotational springs and beams considering nonlinear/linear properties) in predicting kinematics of the ligamentous spine in comparison with a detailed finite element (FE) model while considering various anterior-posterior joint placements. Using the simplified models with different joint offsets in a subject-specific musculoskeletal model, we computed local spinal forces during forward flexion and compared results with intradiscal pressure measurements. In comparison to the detailed FE model, linearized beam and spherical joint models failed to reproduce kinematics whereas the nonlinear beam model with joint offsets at -2 to +4 mm range (+: posterior) showed satisfactory performance. In the musculoskeletal models without a hand-load, removing rotational springs, linearizing passive properties and offsetting the joints posteriorly (by 4 mm) increased compression (~32%, 17% and 11%) and shear (~63%, 26% and 15%) forces. Posterior shift in beam and spherical joints increased extensor muscle active forces but dropped their passive force components resulting in delayed flexion relaxation and lower antagonistic activity in abdominal muscles. Overall and in sagittally symmetric tasks, shear deformable beams with nonlinear properties performed best followed by the spherical joints with nonlinear rotational springs. Using linear rotational springs or beams is valid only in small flexion angles (<30°) and under small external loads. Joints should be placed at the mid-disc height within -2 to +4 mm anterior-posterior range of the disc geometric center and passive properties (joint stiffnesses) should not be overlooked.

Keywords: Musculoskeletal modeling, motion segment, intervertebral joint, spine, finite element

1 Introduction

Under mechanical loads and motions in various daily activities, spinal motion segments display complex nonlinear and transient responses that alter with time, preloads and load/motion directions/magnitudes (Gardner-Morse and Stokes, 2004; Panjabi et al., 1994). Detailed finite element (FE) models, as predictive tools, can satisfactorily replicate these responses in static (Dreischarf et al., 2014; Naserkhaki et al., 2016; Shirazi-Adl, 1994a, b), viscoelastic (Jones and Wilcox, 2008; Wang et al., 2000; Wang et al., 1997) and poroelastic (Argoubi and Shirazi-Adl, 1996; Schmidt et al., 2010; Schroeder et al., 2006) conditions. However, due to the substantial computational burden of such detailed FE models especially in iterative algorithms (Schmidt et al., 2013; Toumanidou and Noailly, 2015), musculoskeletal models of the trunk commonly employ more simplified approaches to take account of the intervertebral joints (including intervertebral discs, ligaments and facet joints) and the spinal passive responses. Proper representation of the intervertebral joints and passive stiffness contributions are crucial in accurate estimation of both muscle forces and hence internal spinal loads and trunk stability margin (Dreischarf et al., 2016). Some models use spherical joints (ball and socket or hinge joints) with fixed centers of rotation along with rotational springs (with linear or nonlinear stiffness properties) (Bruno et al., 2015; Cholewicki and McGill, 1996) while others employ beams (stiffness matrices or bushing elements) that take into account translational degrees of freedom (Christophy et al., 2013; Ignasiak et al., 2016; Malakoutian et al., 2016) and coupled terms as well (El-Rich et al., 2004; Meng et al., 2015; Stokes and Gardner-Morse, 2016). Although foregoing rather simplified models have extensively been employed in earlier studies, their relative accuracy in representing joint kinematics and kinetics remains yet unknown.

Some important concerns regarding these rather simplified models of motion segments include the type of model (beam element versus spherical joint), the use of linear mechanical properties (rotational springs or beams) or none at all (frictionless spherical joints) to simulate passive responses of motion segments and their placement within the spinal joints (cranial-caudal and anterior-posterior). According to the approximation theory, linearizing nonlinear responses of motion segments remains valid only in the neighbourhood of the linearization point, yet the validity domain of utilizing linearized elements has not been explored. Furthermore, some earlier studies carried out sensitivity analyses on the anterior-posterior (Han et al., 2013; Zander et al., 2016) and cranial-caudal (Ghezelbash et al., 2015) positioning of spherical joints and reported marked effects on computed muscle forces and spinal loads. In this regard, changes in the position of the joint center in musculoskeletal models with frictionless spherical joint has been found to have substantial effects on model predictions (Zander et al., 2016). For accurate results, the joint center should coincide with the joint "center-of-reaction" that however neither is known a priori nor remains constant under applied loads and motions (Zander et al., 2016). No comprehensive sensitivity analyses have yet been carried out on the effects of alterations in anterior-posterior positioning of (shear deformable, linear and nonlinear) beam elements or moment resisting spherical joints on predictions of trunk musculoskeletal models.

We, therefore, aim here to investigate the relative performance and accuracy of the simplified models (i.e., spherical joints and shear deformable beams), the effects of using linearized passive properties (instead of the more accurate nonlinear properties) and the role of positioning of the simplified models when predicting trunk kinematics and kinetics. To do so, we initially compare displacements-flexion moment responses of a detailed lumbar spine FE model (Shirazi-Adl, 1994a, b) with those of the simplified models (employing beams or spherical joints with linear and nonlinear stiffness properties). Subsequently, using a validated nonlinear subject-specific FE musculoskeletal model of the trunk (Ghezelbash et al., 2016b), foregoing linear/nonlinear beam elements and spherical joints (representing the entire motion segments) are shifted at all levels in the anterior-posterior direction and muscle forces as well as spinal loads are computed. Estimated intradiscal pressures (IDPs) at the L4-L5 are also compared versus available in vivo measured IDPs (Wilke et al., 2001) during flexed and standing tasks with/without a load in hands. It is hypothesized that the trunk active-passive kinematics-kinetics response is substantially influenced by both the simplification in the model (particularly linear ones) employed and its anterior-posterior position. Based on the characteristic of the center-of-reaction at which no moment resistance exists, it is also hypothesized that for a unique estimation of muscle forces and internal loads as the joint center shifts posteriorly, the simulated passive moment resistance of the motion segments should increase.

2 Methods

Here, we compared passive ligamentous spine (without muscles) responses of simplified models (beams/spherical joints with linear/nonlinear stiffness) versus those of a detailed lumbar spine FE model (Shirazi-Adl, 1994a, b) to determine which simplified approach estimated kinematic responses of the lumbar spine accurately and to identify likely deviations in responses from the detailed FE model. Then, the corresponding musculoskeletal model of each simplified ligamentous spine model were developed by adding the same musculature.

2.1 Ligamentous Spine

To investigate the performance of and accuracy in utilizing beams and moment resisting spherical joints in the trunk musculoskeletal models when simulating the ligamentous spine (isolated spine without muscles), we initially compared their predictions with those (displacements- flexion moment and L1 instantaneous center of rotation (ICoR)) of a detailed lumbar spine FE model (Fig. 1a) under 20 Nm flexion moment and 2.7 kN follower compression load (Shirazi-Adl, 2006). The lumbar spine model (L1 to S1) were previously developed based on CT scans of a cadaver and included intervertebral discs, curved facet surfaces, ligaments and vertebrae (which were modeled each as two rigid bodies interconnected with two deformable beams to account for vertebral compliance) (Shirazi-Adl, 1994a, b). In the beam and spherical joint models, responses were simulated under similar moment and compression follower load (i.e., a load that causes nearly zero vertebral rotations when no moment is applied) passing through beams/spherical joints (from the upper endplate to the lower one) with the L1-L5 vertebrae completely free but the S1 fixed. Simplified models are described as follows:

Nonlinear beam model: In this model (Fig. 1b), vertebrae were assumed rigid and motion segments were replaced with shear deformable beams (representing discs, ligaments and facets) with nonlinear properties running between adjacent vertebral endplate centers (offset=0 mm, Fig. 1d). Nonlinear moment-curvature (level-dependent and different in flexion than in extension) and compression force-strain (level dependent) properties of beams were assigned and verified to match those of the detailed FE model (Shirazi-Adl, 2006) under similar external loading and boundary conditions (see curves in (Ghezelbash et al., 2016b)). Nonlinear moment-curvature and compression force-strain properties of beams were assigned (Shirazi-Adl et al., 2002) and verified to match results of the detailed FE model under similar external loading and boundary conditions (Shirazi-Adl, 2006). Additional models were developed by rigidly shifting beams at all levels perpendicular to their disc mid-height planes (parallel to their reference orientations) (i.e., offset= –2, 2, 4 and 8 mm, Fig. 1d).

Linear beam model: The nonlinear passive properties (moment-curvature and compression force-strain) of the foregoing nonlinear beam model with offset at 4 mm were linearized at and around the origin (up to ~600 N compression and 4 Nm flexion moment) of the load-displacement curves.

Nonlinear spherical joint model: Each beam in the beam models was replaced with a spherical joint (Fig. 1c) placed at its midpoint of corresponding beam when offset=0 mm, Fig. 1d. To account for the nonlinear stiffness of the passive ligamentous spine, we reinforced these joints with nonlinear rotational springs (representing the stiffness of intervertebral discs, ligaments and facet joints) with moment-rotation curves matching those of the detailed FE model (Shirazi-Adl, 2006). Additional models were developed by shifting these joints along the disc mid-height anteriorly by -2 mm or posteriorly by +4 mm.

Linear spherical joint model: The nonlinear rotational springs in the spherical joint model with offset at 4 mm were linearized at and around the origin (up to ~4 Nm flexion moment) of the moment-rotation curve. Translational degrees of freedom are naturally neglected in spherical joint models.

2.2 Musculoskeletal Model

We used our nonlinear subject-specific FE model of the trunk which includes 7 deformable (beams or spherical joints) spinal levels (T11-T12 to L5-S1) and takes account of 126 sagittally-symmetric muscle fascicles to compute muscle forces and spinal loads in an optimization- and kinematics-driven framework (Ghezelbash et al., 2015; Ghezelbash et al., 2016b). At each task, required (reaction) moments at various vertebral levels (T11 to L5) were obtained from the nonlinear FE model. An optimization algorithm estimated muscle forces to minimize the sum of quadratic muscle stresses (as the objective function) along with moment equilibrium equations at all vertebral levels imposed as equality constraints and muscle forces bounded to be greater than the passive force component (Davis et al., 2003) and less than the sum of the passive force component plus $\boldsymbol{PCSA} \times \boldsymbol{\sigma_{max}}$ (where

$\boldsymbol{PCSA}$ and $\boldsymbol{\sigma_{max}}$ = 1 MPa are physiological cross sectional area and maximum muscle stress). At the subsequent iteration, estimated muscle forces were applied to the corresponding vertebra as additional external forces and the iteration repeated until convergence (i.e., muscle forces remaining almost the same in two consequent iterations). Upper body gravity loads were partitioned along the spine (T1 to L5) (Pearsall et al., 1996) as well as arms, head-neck and hands (De Leva, 1996). T11 and S1 rotations were estimated based on sex- and age-specific lumbopelvic rhythm (Pries et al., 2015), and then the total T12-L5 rotations were partitioned by 6.0% at T11–T12, 10.9% at T12- L1, 14.1% at L1–L2, 13.2% at L2–L3, 16.9% at L3–L4, 20.1% at L4–L5, and 18.7% at L5-S1 (Ghezelbash et al., 2016b). Further details on the model and the scaling algorithm are available elsewhere (Ghezelbash et al., 2016b)

Once more here we shifted (rigidly displaced parallel to its reference orientation) nonlinear and linear beams/spherical joints (representing the entire motion segment: disc, ligaments and facets) at all 7 levels (T11-T12 to L5-S1) from 2 mm anterior to -8 mm posterior from the reference position (offset=0 mm, Fig. 1d). Furthermore, as an extreme case, we removed passive elements (rotational springs) and simulated joints as pure frictionless spherical joints with zero offset. In each case, neutral standing posture under gravity alone was initially sought through an optimization process (Shirazi-Adl et al., 2002). Within a kinematics- and optimization-driven framework, muscle forces were then computed in various static standing and forward flexion tasks with/without load (19.8 kg mass) in hands similar to those considered in in vivo studies (Wilke et al., 2001). We evaluated spinal loads using force equilibrium equations and estimated IDPs by employing a quadratic regression equation ($\mathbf{IDP}(\boldsymbol{P},\boldsymbol{\theta}) = -\mathbf{1.556} \times \mathbf{10^{-2}} + \mathbf{1.255}\boldsymbol{P} + \mathbf{1.243} \times \mathbf{10^{-2}}\boldsymbol{\theta} + \mathbf{3.988} \times \mathbf{10^{-2}}\boldsymbol{P^2} - \mathbf{1.212} \times \mathbf{10^{-2}}\boldsymbol{P\theta} + \mathbf{1.669} \times \mathbf{10^{-3}}\boldsymbol{\theta^2}$ where $\boldsymbol{P}$ (MPa) denotes the nominal pressure (compression (N)/total disc cross sectional area (mm^2)) and $\boldsymbol{\theta}$ (°, positive in flexion) is the intersegmental flexion rotation (Ghezelbash et al., 2016b)). After the computation of muscle forces ($\boldsymbol{F}$) during forward flexion, passive ($\boldsymbol{F_p}$) and active ($\boldsymbol{F_a}$) muscle forces of global back muscles were estimated taking $\boldsymbol{F} = \boldsymbol{F_a} + \boldsymbol{F_p}$, with $\boldsymbol{F_p}$ estimated from the muscle elongation (Davis et al., 2003). In the current study, the model was adjusted to fit the subject participated in the IDP measurement study (age= 42, sex=male, body height=173.9 cm and body weight=72 kg) since those personal parameters and particularly the body weight substantially affect spinal loads and hence IDP estimations (Ghezelbash et al., 2016a).

3 Results

Ligamentous **spine:** Under 2700 N follower compression preload and up to 20 Nm flexion moment, L1 (at vertebral center) rotation- and translations-moment responses of the nonlinear beam models~~ in the entire passive L1-S1 lumbosacral model~~ agreed well with those of the detailed FE model (Fig. 2). On the contrary, linear and nonlinear spherical joint models of the passive ligamentous spine deviated from the detailed FE model, particularly in the axial Z-translation (Fig. 2c). In contrast to (linear/nonlinear) spherical joints, the nonlinear beam models with posterior offsets up to +4 mm satisfactorily simulated the path of the L1 centroid, Fig. 3. The instantaneous center of rotation (ICoR) of the L1 was also best simulated by both nonlinear beam elements (correlation coefficient=0.91, mean absolute error of 1.4 mm at -2 mm offset and 3.6 mm at 4 mm offset) as well as the nonlinear spherical joints (correlation coefficient=1.00, mean absolute error of 2.8 mm at -2 mm offset and 4 mm at 4 mm offset) at -2 mm to +4 mm offset; on the other hand, linear spherical joints model (and to a lesser extent the linear beam model) could not replicate the ICoR path either pattern- or magnitude-wise (Fig 3).

Musculoskeletal model: The models and the anterior-posterior placement of joints markedly affected spinal loads, especially under greater flexion angles. Using linear (instead of nonlinear) passive properties increased shear and compression forces, at peak flexion, by 26.3% (174 N) and 17.0% (296 N) in the beam model whereas 18.7% (111 N) and 6.1% (125 N) in the spherical joint model, respectively (Fig. 4). As an extreme case, neglecting passive properties (joint stiffnesses) in the spherical joint model (“No Passive” model in Figs 4-6) substantially increased L5-S1 shear and compression forces (at peak flexion by 63.0% and 32.3% or equivalently by 330 N and 665 N, respectively), Fig. 4. At the joint offset of +4 mm and in forward flexion, estimated L5-S1 local compression and shear forces increased from their values at the reference case (i.e., 0 mm) by as much as 10.9% and 15.7% in the nonlinear beam model, and 11.4% and 12.4% in the nonlinear spherical joint model, respectively (Fig. 4). Likewise and in accordance with the variations in computed compression forces, when linearized passive properties were utilized (or neglected in the spherical joint model) and when the joints shifted posteriorly, the estimated IDPs markedly increased especially in the heavier tasks with load in hands (Fig. 5). Location of joint in both beam and spherical joints substantially affected the force partitioning between passive and active muscle components. As joints shifted posteriorly, the active component of back muscles increased (e.g., by 137 N in the global iliocostalis muscle) while at the same time the passive component dropped (e.g., by 107 N in the global iliocostalis muscle) (Fig. 6).

4 Discussion

In the current study, we explored the relative performance and validity of various rather simplified models of spinal motion segments regularly used in trunk musculoskeletal models. In particular, spherical joints were compared to beam elements using matched linear and nonlinear stiffness properties with locations varying from the anterior to the posterior of the disc geometric centers. The predictions were compared in a ligamentous lumbar spine model versus a detailed L1-S1 FE model under follower compression and flexion moment and in a trunk musculoskeletal model in forward flexion with and without load in hands versus reported in vivo disc pressure measurements. Equivalent stiffness properties of nonlinear beam as well as spherical joint models were initially set by matching global displacements under combined flexion-compression with those of an existing detailed FE model. Hypotheses were confirmed in finding substantial effects of modeling, especially when using linear stiffness properties or no stiffness at all in frictionless spherical joints, and joint position on spine kinematics and kinetics. Muscle forces and spinal loads increased as joints shifted posteriorly. Finally, for identical predictions on muscle forces and spinal loads, one is needed to increase passive properties (joint stiffnesses) to counterbalance the added moment of external/gravity loads as well as the reduced resisting moment of back muscles as joint position shifts posteriorly.

Limitations: Kinematics were matched only under flexion moments up to 20 Nm in the presence of a 2700 N follower compression preload. While considering the stiffening role of the compressive preload in flexion (Shirazi-Adl, 2006; Stokes et al., 2002) and the nonlinear responses in flexion and compression, the employed nonlinear shear deformable beam model should be considered only as a rather simplified replicate of a detailed FE model of the motion segment. Nonlinear beam and spherical joint musculoskeletal models with the offsets at 0 (in peak flexion and for the spherical joint only) and -2 mm (in 90º and peak flexions) did not converge due to excessive flexion moments at the lower lumbar levels. Likewise, linearized models did not converge in upright posture holding a 19.8kg load away. The current study focused only on sagittally symmetric tasks (both posture and loading). Although nonlinear beam and spherical joint models demonstrated satisfactory performances in such conditions, extension of findings to asymmetric tasks should await future studies. Presented results with alterations at all levels cannot identify the relative effects of changes in individual segments on results that would require a sensitivity analyses on each joint positioning. Other limitations and shortcomings related to the musculoskeletal modeling are presented elsewhere (Arjmand and Shirazi-Adl, 2006; Ghezelbash et al., 2015; Shahvarpour et al., 2015).

Interpretation and comparison: Unlike the nonlinear beam model, the nonlinear spherical joint model did not as accurately predict cranial-caudal translation (Fig. 2c) ~~and ICoR of the L1 (Fig. 3)~~ due to the lack of translational degrees of freedom. This model overlooks the compliances under shear and axial compression forces and as such its response predictions deteriorate further under greater loads. Another variable in spherical joint modeling, unlike the beam simulation, is the cranial-caudal location of the joint. Here we placed these joints at the disc mid-heights at all levels and analyses. Our earlier studies, however, demonstrated that changing the center of spherical joints from the mid-disc height in the cranial-caudal direction within upper and lower endplates would yield up to ~15% and ~30% differences in the computed compression and shear forces, respectively (Ghezelbash et al., 2015).

Posterior joint offsets in both beam and spherical joints locations in the musculoskeletal models substantially affected muscle forces and spinal loads. For example, L5-S1 spinal loads increased up to 20.1% in compression and 23.1% in shear as the beam shifted from the disc center posteriorly by 8 mm. Spinal loads however dropped by 9.7% and 18.2% as the joint shifted anteriorly by 2 mm. Foregoing alterations in muscle forces and spinal loads are due directly to the combined effects of changes in the net external moments, lever arms of muscles evaluated at the updated position of joints and alterations in extensor muscle passive forces. As the joint (beam or spherical model) shifts posteriorly, the net external moment of gravity and load in hands increase while the lever arm of extensor muscles decrease resulting both in larger muscle forces and hence spinal loads. Reverse trends occur as the joint shifts anteriorly instead. At flexion>70º, increases in muscle lengths and thus passive muscle forces noticeably decreased as joints shifted posteriorly (Fig. 6), and since at full flexion, passive muscle forces are a major contributor to spinal loads, computed IDPs at full flexion by different beam models remained almost the same (Fig. 5). In agreement with our findings, Zander et al. (2016) and Han et al. (2013) also computed larger (smaller) spinal loads when joints shifted posteriorly (anteriorly).

In other words and as schematically illustrated in Fig. 6, when joint locations shift posteriorly at all levels (from point 1 to 2 or 3), muscle forces increased resulting in larger compression forces. Alternatively and in order to keep muscle forces and hence joint loads at constant magnitudes irrespective of the joint location, passive resistance of the joint should increase as the joint location shifts posteriorly. This condition is shown in Fig. 7 where although there is no internal moment required when the joint center instantaneously coincides with the joint "center-of-reaction", the internal resistant moment should increase as the joint center shifts from the point 1 to 2 and further to 3; $M_3 > M_2 > M_1 \sim 0$. In addition and compared to the beam model at identical locations, the spherical joint model even with nonlinear properties overestimated compression forces (or equivalently IDPs) in demanding tasks (e.g., lifting 19.8 kg load at flexion 70º, Fig. 5) due mainly to overlooking the stiffening role of the compressive force on the passive responses. Neglecting this factor particularly in demanding tasks reduced the load-carrying role of the passive spine and increased muscle activities (Arjmand and Shirazi-Adl, 2005). Overall, best agreements were found in beam models with smaller joint offsets. In this study, we shifted joints along the corresponding disc mid-height plane, which is more reasonable. Additional analyses with joint offsets carried out in global horizontal direction (X) did however demonstrate only negligible changes in spinal forces (<1% smaller in compression and <4% greater in shear).

Variations in joint offset altered spinal kinematics and therefore active-passive muscle force partitioning and net moment resistant contributions. As joints shifted anteriorly, net moments and the active component of back muscles both decreased (Fig. 6); thus, at early- to mid-flexion points, larger spinal loads in models with posteriorly placed joints were mainly due to larger active components in muscle forces. However, anterior joint placement also markedly increased the elongation in extensor muscles and hence their passive forces (Fig. 6) so much so that at flexions>70º, these passive muscle forces and resulting spinal loads increased significantly in models at greater anterior offsets counterbalancing the effects of reduction in active muscle forces (Figs 5, 6). Featured by a substantial drop in extensor muscle activities, flexion-relaxation angle (defined as the trunk forward flexion at which extensor muscles become silent) was delayed from ~60º to ~90º as joints shifted from -2 to 8 mm. This occurred since anterior offset in joints tended to substantially and concurrently increase passive but decrease active force contributions of back muscles. It is interesting to note that, in counterbalancing the excessive resistant moment generated by large passive forces in extensor muscles, anterior disc offset tends also to further increase antagonistic activities in abdominal muscles initiated in larger trunk flexion angles.

Linearization of passive properties as an approximation of the nonlinear response remains valid only in the neighborhood of the linearization point. The further one deviates from the reference linearization point; the more divergence is expected in results away from the original nonlinear system; thus, using linear passive properties (constant joint stiffnesses) (as the mainstream modeling technique (Bruno et al., 2017; De Zee et al., 2007; Delp et al., 2007)) seems reasonable only in a small range. At the extreme in the frictionless spherical joint with no passive resistance, due to marked load-carrying role of the passive ligamentous spine, muscles alone will resist the moments of external loads resulting in greater muscle forces and internal loads, especially in heavier tasks with larger trunk rotations. Thus, in musculoskeletal modeling software (such as AnyBody and OpenSim (Christophy et al., 2012; De Zee et al., 2007; Delp et al., 2007)), we recommend to use nonlinear intervertebral joint stiffness in tasks with large flexion angles (>40º) or to use linear joint stiffness only when flexion angles remain relatively small (<40º). One valid but cumbersome alternative option is to continuously update the linear stiffness properties depending on the current load magnitude considered in an analysis. Passive elements (rotational springs) should however never be neglected.

One should consider both kinematics and kinetics of the spine and their likely interactions while positioning intervertebral joints. To accurately capture kinematics responses, one can place spherical joints at or near corresponding ICoRs; however, according to the current and earlier (Ghezelbash et al., 2015) results, using reported ICoR values (e.g., ~ 16 mm posterior to disc centers (Liu et al., 2016) or near lower endplates (Staub et al., 2015)) without proper adjustments in passive properties (joint stiffnesses) adversely influences the kinetics (i.e., muscle forces and spinal loads). During flexion and relative to the lower vertebra, a spherical joint considers a fixed ICoR whereas a shear deformable beam accounts for some translations in ICoR. (~ 0.6 mm during flexion under 2.7 kN follower preload). In this study, the simplified nonlinear models estimated the ICoR locus of the L1 fairly well during its overall (global) motion. It should be noted that the center of rotation (i.e., a point that has no instantaneous velocity under applied loads) does not fall on the "center of reaction" (i.e., a point in which the net moment vanishes (Gracovetsky et al., 1987; Zander et al., 2016), so moment equilibrium equations about the center of rotation should not overlook the internal moment (Fig. 6). Alternatively, one can write equilibrium equations about the "center of reaction" with no net (internal) moment. Although the "center of reaction" introduces significant computational simplicity, this point is not known a priori and displaces during deformation.

Results of this study have implications in biomechanics of total disc replacements that should be considered in future designs. Anterior-posterior placement of these implants, passive resistance they offer and the nonlinearity in their stiffnesses under increasing compression and rotations should be carefully considered and examined as they all influence spinal kinematics, muscle forces and hence internal loads.

In summary, we explored the accuracy and validity, in sagittally symmetric tasks, of modeling spinal motion segments as spherical joints (with and without rotational springs) and beams both with linear/nonlinear passive properties while their location shifted in the anterior-posterior directions. Estimated kinematics by these simplified models (spherical joint/beam) were compared with a detailed FE model of the lumbar spine under a

2.7 kN follower load and 20 Nm moment. Introducing foregoing simplified models into a subject-specific musculoskeletal model, we predicted active-passive components of muscle forces and local spinal loads at various lifting tasks and compared the computed IDP with available in vivo measurements (Wilke et al., 2001). Nonlinear shear deformable beams and nonlinear spherical joints with joint offset at -2 to 4 mm range predicted kinematics (in comparison with the detailed FE) and spinal loads (in comparison with the in vivo measurements) accurately although the nonlinear spherical joint model failed to accurately estimate the axial displacements. Shifting joints posteriorly in general increased spinal loads (up to 17% in compression and 26% in shear) and delayed flexion relaxation (by 40^{o}) during forward flexion. Employing linear rotational springs or beams remained valid only at relatively small flexion angles ($<40^{o}$). Due to the substantial role of the ligamentous spine in resisting external moments especially in heavier tasks, overlooking rotational springs (i.e., in frictionless spherical joints) should be avoided as it would yield marked overestimation of compression (32%) and shear (63%) forces.

5 Acknowledgments

This work was supported by the institut de recherche Robert-Sauvé en santé et en sécurité du travail (IRSST-2014-0009) and fonds de recherche du Québec en nature et technologies (FRQNT-200564).

6 Conflict of Interest

Authors have no conflict of interest to declare.

7 References

Argoubi, M., Shirazi-Adl, A., 1996. Poroelastic creep response analysis of a lumbar motion segment in compression. Journal of biomechanics 29, 1331-1339.

Arjmand, N., Shirazi-Adl, A., 2005. Biomechanics of changes in lumbar posture in static lifting. Spine 30, 2637-2648.

Arjmand, N., Shirazi-Adl, A., 2006. Model and in vivo studies on human trunk load partitioning and stability in isometric forward flexions. J Biomech 39, 510-521.

Bruno, A.G., Bouxsein, M.L., Anderson, D.E., 2015. Development and validation of a musculoskeletal model of the fully articulated thoracolumbar spine and rib cage. Journal of biomechanical engineering 137, 081003.

Bruno, A.G., Mokhtarzadeh, H., Allaire, B.T., Velie, K.R., De Paolis Kaluza, M., Anderson, D.E., Bouxsein, M.L., 2017. Incorporation of CT-based measurements of trunk anatomy into subject-specific musculoskeletal models of the spine influences vertebral loading predictions. Journal of Orthopaedic Research.

Cholewicki, J., McGill, S.M., 1996. Mechanical stability of the in vivo lumbar spine: implications for injury and chronic low back pain. Clin Biomech 11, 1-15.

Christophy, M., Curtin, M., Senan, N.A.F., Lotz, J.C., O'Reilly, O.M., 2013. On the modeling of the intervertebral joint in multibody models for the spine. Multibody System Dynamics 30, 413-432.

Christophy, M., Senan, N.A.F., Lotz, J.C., O'Reilly, O.M., 2012. A musculoskeletal model for the lumbar spine. Biomec Model Mechan 11, 19-34.

Davis, J., Kaufman, K.R., Lieber, R.L., 2003. Correlation between active and passive isometric force and intramuscular pressure in the isolated rabbit tibialis anterior muscle. J Biomech 36, 505-512.

De Leva, P., 1996. Adjustments to Zatsiorsky-Seluyanov's segment inertia parameters. J Biomech 29, 1223-1230.

De Zee, M., Hansen, L., Wong, C., Rasmussen, J., Simonsen, E.B., 2007. A generic detailed rigid-body lumbar spine model. J Biomech 40, 1219-1227.

Delp, S.L., Anderson, F.C., Arnold, A.S., Loan, P., Habib, A., John, C.T., Guendelman, E., Thelen, D.G., 2007. OpenSim: open-source software to create and analyze dynamic simulations of movement. IEEE T Bio-Med Eng 54, 1940-1950.

Dreischarf, M., Shirazi-Adl, A., Arjmand, N., Rohlmann, A., Schmidt, H., 2016. Estimation of loads on human lumbar spine: a review of in vivo and computational model studies. Journal of biomechanics 49, 833-845.

Dreischarf, M., Zander, T., Shirazi-Adl, A., Puttlitz, C., Adam, C., Chen, C., Goel, V., Kiapour, A., Kim, Y., Labus, K., 2014. Comparison of eight published static finite element models of the intact lumbar spine: Predictive power of models improves when combined together. J Biomech 47, 1757-1766.

El-Rich, M., Shirazi-Adl, A., Arjmand, N., 2004. Muscle activity, internal loads, and stability of the human spine in standing postures: combined model and in vivo studies. Spine 29, 2633-2642.

Gardner-Morse, M.G., Stokes, I.A., 2004. Structural behavior of human lumbar spinal motion segments. Journal of Biomechanics 37, 205-212.

Ghezelbash, F., Arjmand, N., Shirazi-Adl, A., 2015. Effect of intervertebral translational flexibilities on estimations of trunk muscle forces, kinematics, loads, and stability. Comput Method Biomec 18, 1760-1767.

Ghezelbash, F., Shirazi-Adl, A., Arjmand, N., El-Ouaaid, Z., Plamondon, A., 2016a. Effects of sex, age, body height and body weight on spinal loads: sensitivity analyses in a subject-specific trunk musculoskeletal model. J Biomechanics.

Ghezelbash, F., Shirazi-Adl, A., Arjmand, N., El-Ouaaid, Z., Plamondon, A., 2016b. Subject-specific biomechanics of trunk: musculoskeletal scaling, internal loads and intradiscal pressure estimation. Biomechanics and modeling in mechanobiology, 1-14.

Gracovetsky, S., Zeman, V., Carbone, A., 1987. Relationship between lordosis and the position of the centre of reaction of the spinal disc. Journal of biomedical engineering 9, 237-248.

Han, K.-S., Kim, K., Park, W.M., Lim, D.S., Kim, Y.H., 2013. Effect of centers of rotation on spinal loads and muscle forces in total disk replacement of lumbar spine. Proceedings of the Institution of Mechanical Engineers, Part H: Journal of Engineering in Medicine 227, 543-550.

Ignasiak, D., Dendorfer, S., Ferguson, S.J., 2016. Thoracolumbar spine model with articulated ribcage for the prediction of dynamic spinal loading. Journal of biomechanics 49, 959-966.

Jones, A.C., Wilcox, R.K., 2008. Finite element analysis of the spine: towards a framework of verification, validation and sensitivity analysis. Medical engineering & physics 30, 1287-1304.

Liu, Z., Tsai, T.-Y., Wang, S., Wu, M., Zhong, W., Li, J.-S., Cha, T., Wood, K., Li, G., 2016. Sagittal plane rotation center of lower lumbar spine during a dynamic weight-lifting activity. Journal of biomechanics 49, 371-375.

Malakoutian, M., Street, J., Wilke, H.-J., Stavness, I., Fels, S., Oxland, T., 2016. A musculoskeletal model of the lumbar spine using ArtiSynth–development and validation. Computer Methods in Biomechanics and Biomedical Engineering: Imaging & Visualization, 1-8.

Meng, X., Bruno, A.G., Cheng, B., Wang, W., Bouxsein, M.L., Anderson, D.E., 2015. Incorporating six degree-of-freedom intervertebral joint stiffness in a lumbar spine musculoskeletal model-method and performance in flexed postures. J Biomech Eng-T ASME 137, 101008.

Naserkhaki, S., Jaremko, J.L., Adeeb, S., El-Rich, M., 2016. On the load-sharing along the ligamentous lumbosacral spine in flexed and extended postures: Finite element study. Journal of biomechanics 49, 974-982.

Panjabi, M.M., Oxland, T., Yamamoto, I., Crisco, J., 1994. Mechanical behavior of the human lumbar and lumbosacral spine as shown by three-dimensional load-displacement curves. The Journal of Bone & Joint Surgery 76, 413-424.

Pearsall, D.J., Reid, J.G., Livingston, L.A., 1996. Segmental inertial parameters of the human trunk as determined from computed tomography. Ann Biomed Eng 24, 198-210.

Pries, E., Dreischarf, M., Bashkuev, M., Putzier, M., Schmidt, H., 2015. The effects of age and gender on the lumbopelvic rhythm in the sagittal plane in 309 subjects. J Biomech 48, 3080-3087.

Schmidt, H., Galbusera, F., Rohlmann, A., Shirazi-Adl, A., 2013. What have we learned from finite element model studies of lumbar intervertebral discs in the past four decades? Journal of biomechanics 46, 2342-2355.

Schmidt, H., Shirazi-Adl, A., Galbusera, F., Wilke, H.-J., 2010. Response analysis of the lumbar spine during regular daily activities—a finite element analysis. Journal of biomechanics 43, 1849-1856.

Schroeder, Y., Wilson, W., Huyghe, J.M., Baaijens, F.P., 2006. Osmoviscoelastic finite element model of the intervertebral disc. European spine journal 15, 361-371.

Shahvarpour, A., Shirazi-Adl, A., Larivière, C., Bazrgari, B., 2015. Trunk active response and spinal forces in sudden forward loading–analysis of the role of perturbation load and pre-perturbation conditions by a kinematics-driven model. J Biomech 48, 44-52.

Shirazi-Adl, A., 1994a. Biomechanics of the lumbar spine in sagittal/lateral moments. Spine 19, 2407-2414.

Shirazi-Adl, A., 1994b. Nonlinear stress analysis of the whole lumbar spine in torsion—mechanics of facet articulation. J Biomech 27, 289-299.

Shirazi-Adl, A., 2006. Analysis of large compression loads on lumbar spine in flexion and in torsion using a novel wrapping element. J Biomech 39, 267-275.

Shirazi-Adl, A., Sadouk, S., Parnianpour, M., Pop, D., El-Rich, M., 2002. Muscle force evaluation and the role of posture in human lumbar spine under compression. Eur Spine J 11, 519-526.

Staub, B.N., Holman, P.J., Reitman, C.A., Hipp, J., 2015. Sagittal plane lumbar intervertebral motion during seated flexion-extension radiographs of 658 asymptomatic nondegenerated levels. Journal of Neurosurgery: Spine 23, 731-738.

Stokes, I.A., Gardner-Morse, M., 2016. A database of lumbar spinal mechanical behavior for validation of spinal analytical models. Journal of biomechanics 49, 780-785.

Stokes, I.A., Gardner-Morse, M., Churchill, D., Laible, J.P., 2002. Measurement of a spinal motion segment stiffness matrix. Journal of Biomechanics 35, 517-521.

Toumanidou, T., Noailly, J., 2015. Musculoskeletal Modeling of the Lumbar Spine to Explore Functional Interactions between Back Muscle Loads and Intervertebral Disk Multiphysics. Frontiers in bioengineering and biotechnology 3.

Wang, J.-L., Parnianpour, M., Shirazi-Adl, A., Engin, A.E., 2000. Viscoelastic finite-element analysis of a lumbar motion segment in combined compression and sagittal flexion: Effect of loading rate. Spine 25, 310-318.

Wang, J., Parnianpour, M., Shirazi-Adl, A., Engin, A., Li, S., Patwardhan, A., 1997. Development and validation of a viscoelastic finite element model of an L2/L3 motion segment. Theoretical and applied fracture mechanics 28, 81-93.

Wilke, H.-J., Neef, P., Hinz, B., Seidel, H., Claes, L., 2001. Intradiscal pressure together with anthropometric data–a data set for the validation of models. Clin Biomech 16, S111-S126.

Zander, T., Dreischarf, M., Schmidt, H., 2016. Sensitivity analysis of the position of the intervertebral centres of reaction in upright standing–a musculoskeletal model investigation of the lumbar spine. Medical Engineering & Physics 38, 297-301.

Figure Captions

Fig. 1: Schematic illustration of the (a) detailed FE model (with intervertebral disc, facet joints and ligaments at all levels), (b) beam model, (c) spherical joint model and (d) beam positioning and offset (+ posterior; - anterior) at a typical motion segment.

Fig. 2: (a) Flexion rotation, (b) X-translation and (c) Z- translation (see Fig. 3 for axes) of the L1 vertebra in different models (detailed FE, beam and spherical joint) under 20 Nm flexion moment and 2700 N follower preload. Values in parentheses denote joint offset (+ posterior; -anterior) (see Fig. 1d).

Fig. 3: Path of the center the L1 (left) and ICoR of the L1 (right) during forward flexion (from right to left) for different joint types and offset magnitudes

Fig. 4: Computed local L5-S1 compression (left) and shear (right) forces in different flexed postures without hand load for different joint types and offset values (+ posterior; - anterior) (see Fig.1d). Personal parameters of the model were set at sex=male, body height=173.9 cm, body weight=72.0 kg and age=42.0 years. Values in the parentheses denote joint offset (+ posterior; -anterior).

Fig. 5: Measured (Wilke et al., 2001) and estimated IDPs (using the compression-IDP-flexion rottaion relation proposed in (Ghezelbash et al., 2016b)) during various tasks. Values in the parentheses denote joint offset (+ posterior; -anterior) (see Fig. 1d).

Fig. 6: Active and passive muscle force components in right/left global longissimus (left) and iliocostalis (right) pars thoracic muscles during forward flexion with no load in hands in the nonlinear beam model at different offsets (see Fig. 1d). Drop and disappearance of active muscle forces denote the flexion relaxation phenomenon in forward flexion.

Fig. 7: Schematic illustration of joint positioning kinetics. W: external (in hands) and gravity forces; F: extensor muscle forces; M_1, M_2 and M_3: resultant free-body diagram moments at the plane of cut (M_1<M_2<M_3)

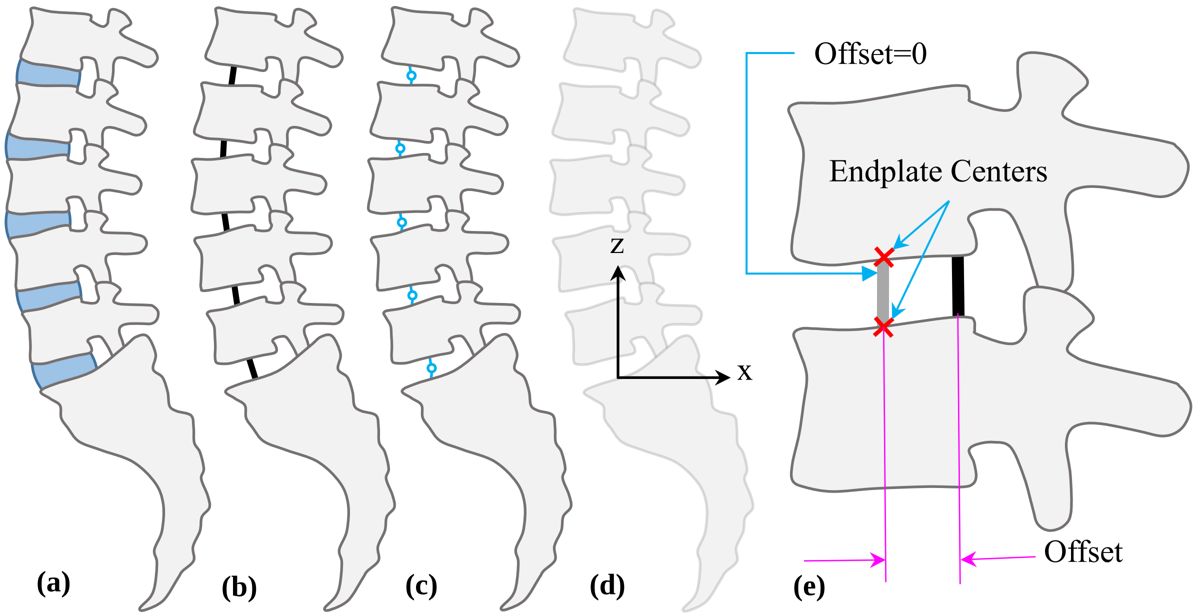

Fig. 1

Fig. 2

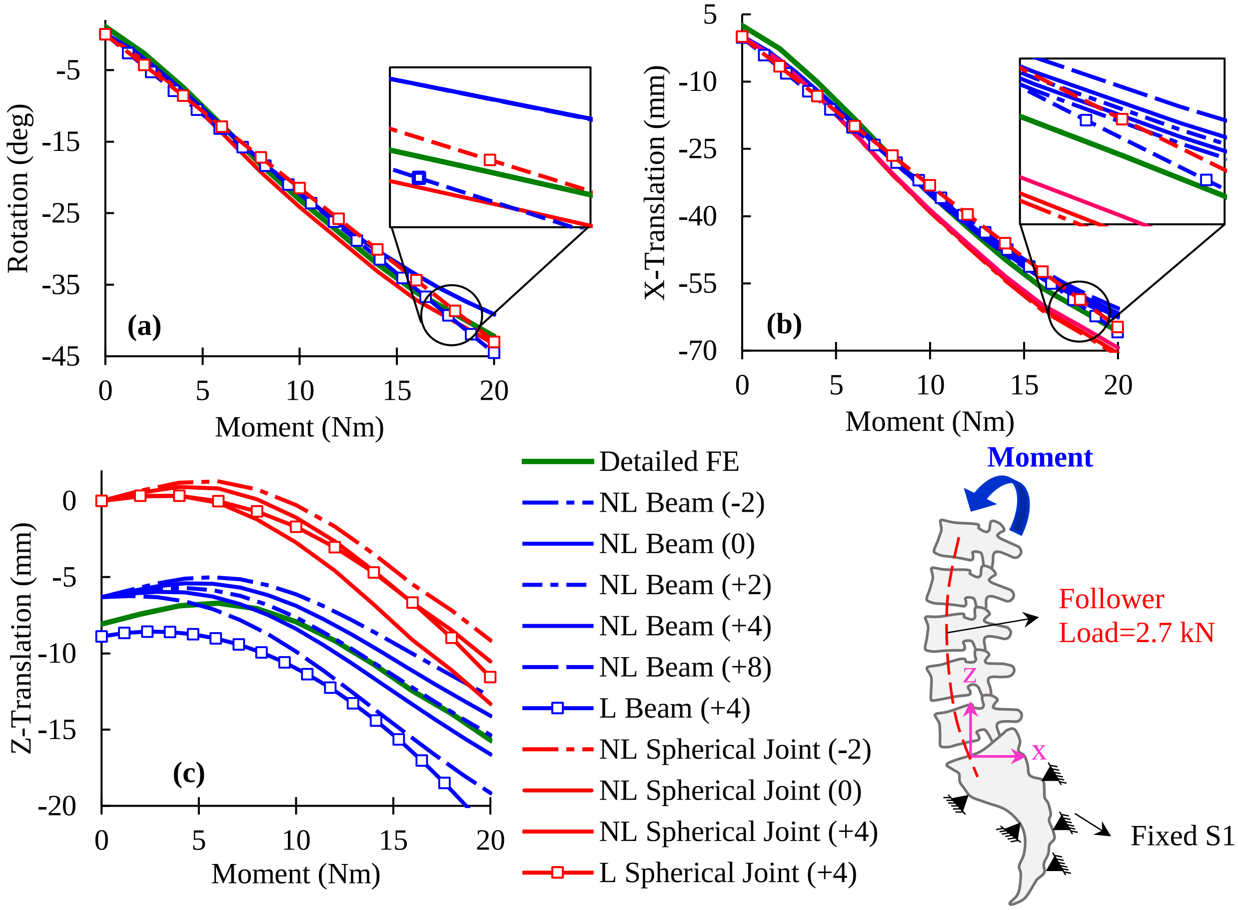

(a)
Rotation (deg)
Moment (Nm)
(b)
X-Translation (mm)
Moment (Nm)
(c)
Z-Translation (mm)
Moment (Nm)
Detailed FE
NL Beam (-2)
NL Beam (0)
NL Beam (+2)
NL Beam (+4)
NL Beam (+8)
L Beam (+4)
NL Spherical Joint (-2)
NL Spherical Joint (0)
NL Spherical Joint (+4)
L Spherical Joint (+4)
Moment
Follower
Load=2.7 kN
z
x
Fixed S1

Fig. 3

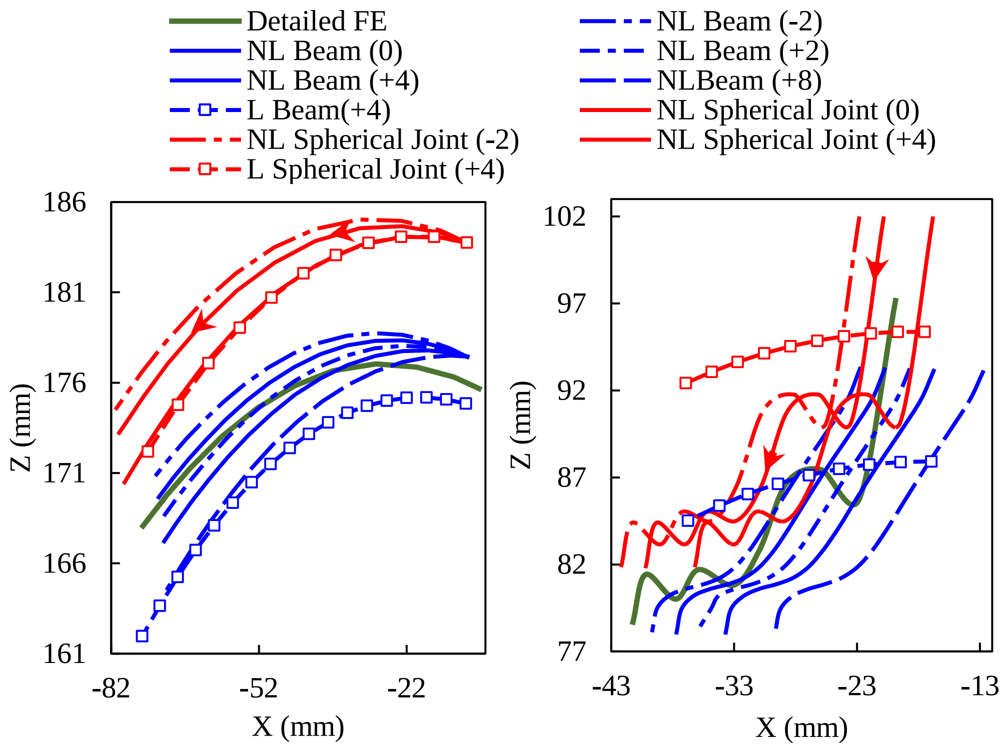

Detailed FE
NL Beam (0)
NL Beam (+4)
L Beam(+4)
NL Spherical Joint (-2)
L Spherical Joint (+4)
NL Beam (-2)
NL Beam (+2)
NLBeam (+8)
NL Spherical Joint (0)
NL Spherical Joint (+4)
186
181
176
171
166
161
Z (mm)
-82
-52
-22
X (mm)
102
97
92
87
82
77
Z (mm)
-43
-33
-23
-13
X (mm)

Fig. 4

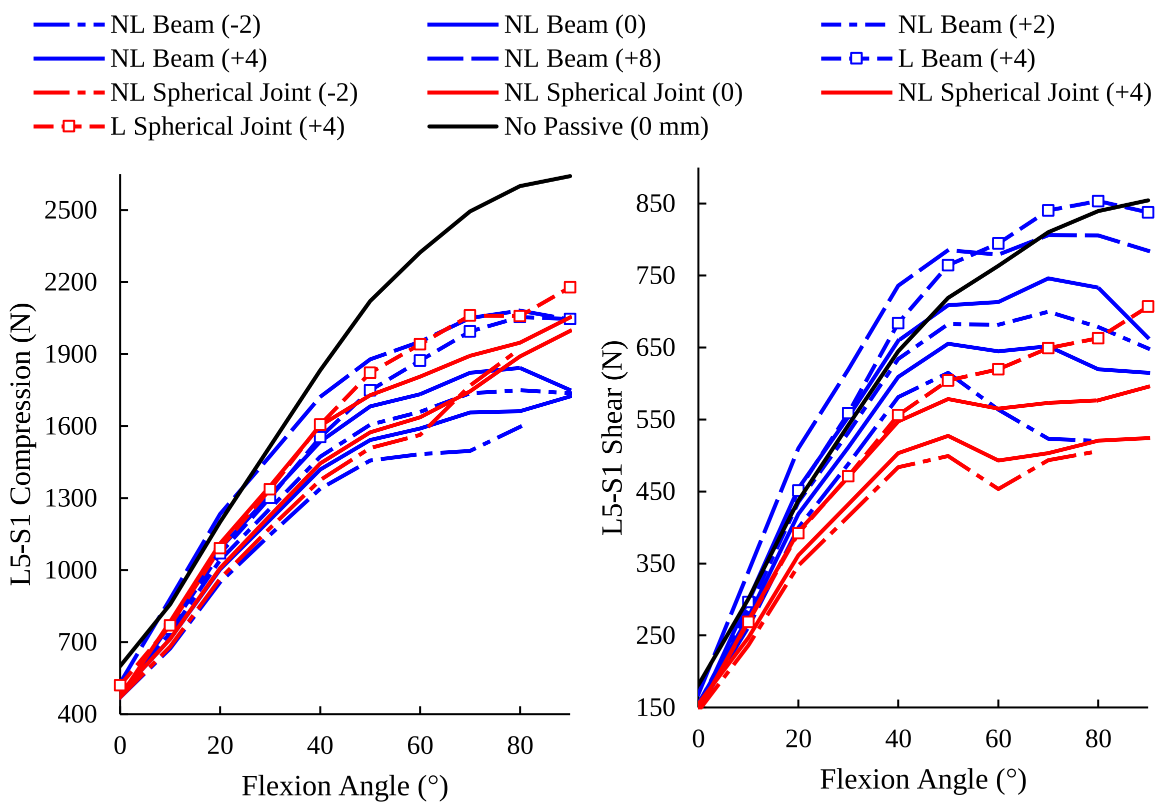

NL Beam (-2)
NL Beam (0)
NL Beam (+2)
NL Beam (+4)
NL Beam (+8)
L Beam (+4)
NL Spherical Joint (-2)
NL Spherical Joint (0)
NL Spherical Joint (+4)
L Spherical Joint (+4)
No Passive (0 mm)
L5-S1 Compression (N)
2500
2200
1900
1600
1300
1000
700
400
0
20
40
60
80
Flexion Angle (°)
L5-S1 Shear (N)
850
750
650
550
450
350
250
150
0
20
40
60
80
Flexion Angle (°)

Fig. 5

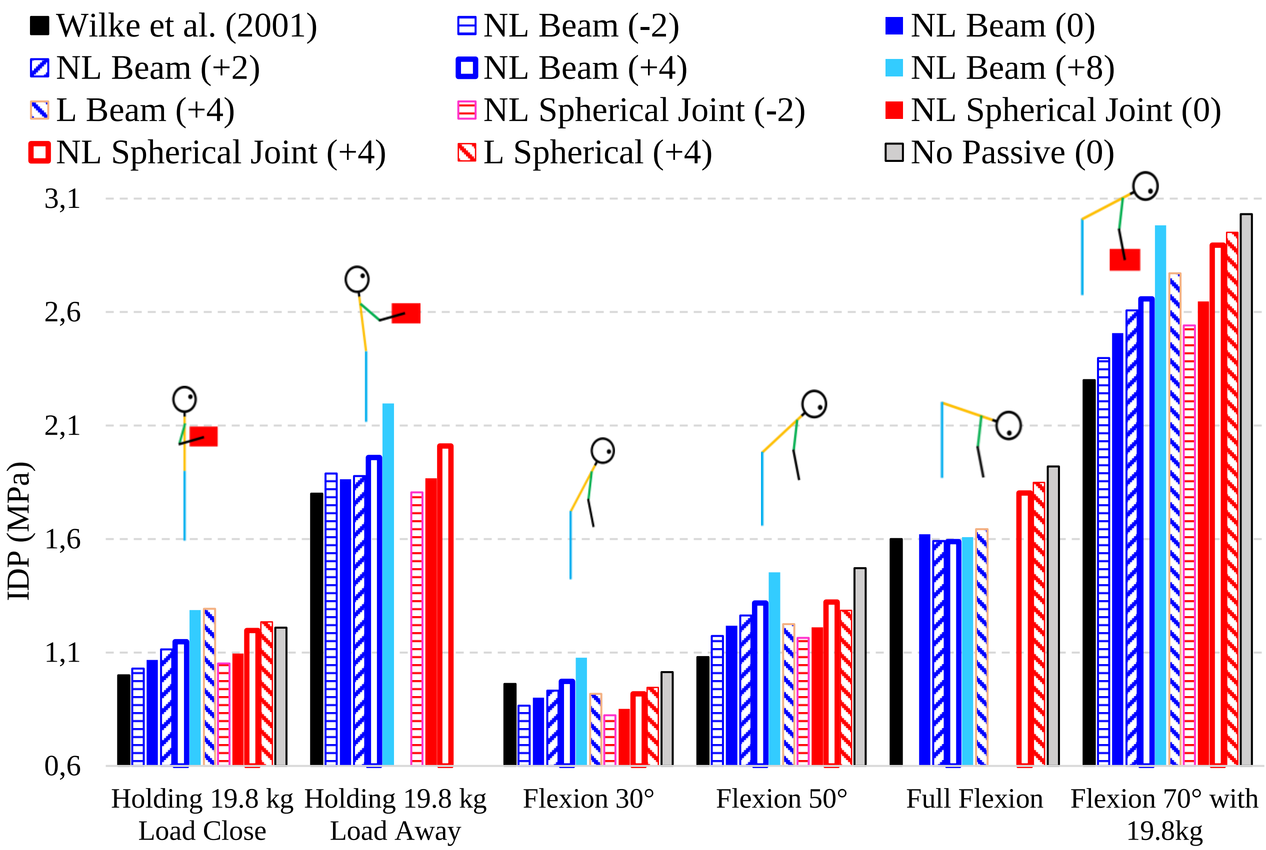

Wilke et al. (2001)
NL Beam (-2)
NL Beam (0)
NL Beam (+2)
NL Beam (+4)
NL Beam (+8)
L Beam (+4)
NL Spherical Joint (-2)
NL Spherical Joint (0)
NL Spherical Joint (+4)
L Spherical (+4)
No Passive (0)
IDP (MPa)
3,1
2,6
2,1
1,6
1,1
0,6
Holding 19.8 kg Load Close
Holding 19.8 kg Load Away
Flexion 30°
Flexion 50°
Full Flexion
Flexion 70° with 19.8kg

Fig. 6

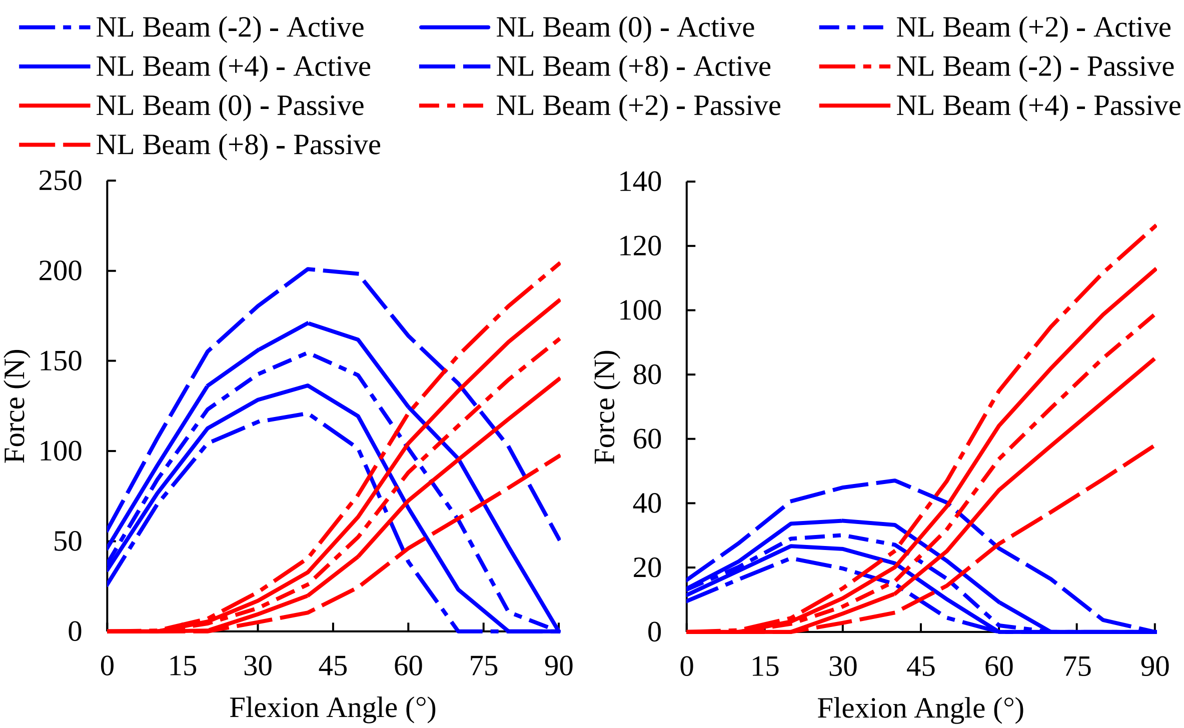
NL Beam (-2) - Active
NL Beam (0) - Active
NL Beam (+2) - Active
NL Beam (+4) - Active
NL Beam (+8) - Active
NL Beam (-2) - Passive
NL Beam (0) - Passive
NL Beam (+2) - Passive
NL Beam (+4) - Passive
NL Beam (+8) - Passive
Force (N)
0
50
100
150
200
250
0
15
30
45
60
75
90
Flexion Angle (°)
Force (N)
0
20
40
60
80
100
120
140
0
15
30
45
60
75
90
Flexion Angle (°)

Fig. 7

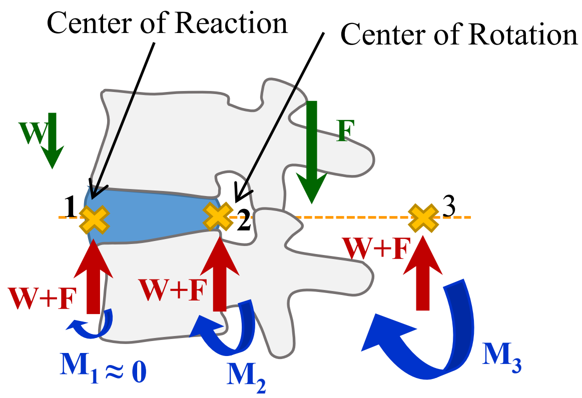
Center of Reaction
Center of Rotation
W
F
1
2
3
W+F
W+F
W+F
M1 ≈ 0
M2
M3